Acta Cybernetica **26** (2024) 799–816.

Robust Control and Actuator Fault Detection Based on an Iterative LMI Approach: Application on a Quadrotor

Oussama Benzinane[ab] and Andreas Rauh[ac]

Abstract

Linear Matrix Inequalities (LMIs) have recently gained momentum due to the increasing performance of computing hardware. Many current research activities rely on the advantages of this growth in order to design controllers with provable stability and performance guarantees. To guarantee robustness despite actuator faults, model uncertainty, nonlinearities, and measurement noise, a novel iterative LMI approach is presented to design an observer-based state feedback controller allowing for simultaneous optimization of the control and observer gains. A comparison with a combination of an Extended Kalman Filter (EKF) and a Linear-Quadratic Regulator (LQR) has been conducted, inherently providing guaranteed stability for the closed loop only when the separation principle holds, which is not the case in this study. Both approaches are applied on a quadrotor, where reliable detection and compensation of the faults in the presence of measurement noise is demonstrated.

Keywords: robust control, linear matrix inequalities, interval methods, extended Kalman Filter, linear-quadratic regulator

1 Introduction

Stability, robustness, and fault tolerance are the most challenging purposes that the researchers have tackled by developing different control and estimation techniques. One of the domains of application is aeronautics, where flight control systems play a major role in ensuring the safety of drones when tracking desired trajectories. During the flight, quadrotors face many issues that originate from the inside (such as a suddenly broken rotor or a failed transmission of measurements from GPS) or from the surrounding environment (e.g., lateral wind). Unavoidably, detection and compensation of faults should take place to reduce the effects of such issues.

[a]Distributed Control in Interconnected Systems, Carl von Ossietzky Universität Oldenburg, Germany
[b]ORCID: 0000-0002-8633-1139
[c]E-mail: andreas.rauh@uni-oldenburg.de, ORCID: 0000-0002-1548-6547

DOI: 10.14232/actacyb.301392

In the literature, see [1], [7], [2] and [16], many researchers have exploited benefits of fault-tolerant methods. Particularly, some attention has been paid to the use of the LMI approach for detecting and compensating actuator faults. For instance, in the paper [12], the authors have investigated the LMI approach to reconfigure the controller parameters for a discrete-time switched system in the presence of actuator faults, unstructured uncertainties, and time delay.

Since systems in the real world are nonlinear, the use of a linear control system, tuned for a single operating point, might not ensure stability and performance. Hence, reformulating the modeled nonlinear system into a quasi-linear form, and based on this, into a polytopic representation with bounded parameter uncertainty allows for exploiting LMI approaches during the design of the control system. In [11], the authors have presented a joint optimization of the combination of control laws and filters taking into consideration bounded uncertainty and noise. In [10], the authors have developed a strategy for desensitization of the closed-loop behavior towards stochastic noise in continuous-time scenarios. Then, exploiting the ideas published in the paper [4], the present paper constitutes a contribution to the design of a discrete-time observer-based state feedback controller in the presence of both bounded parameter uncertainty and stochastic noise in order to guarantee robust performance despite actuator faults, model uncertainty, nonlinearities, and measurement noise. The proposed design procedure allows for optimizing controller and observer gains simultaneously. It consists of the following two phases: (i) placement of poles into a desired area within the complex z-plane and (ii) desensitization of the closed loop to stochastic noise.

From the literature, a huge amount of research has been conducted to exploit the Extended Kalman Filter (EKF) to accurately estimate state variables. Moreover, they are often combined with linear-quadratic regulators (LQR) c.f. [8] and [15]. Hence, for the purpose of comparison, the actuator faults are not only estimated in this paper but also using the EKF. To compensate the actuator faults and for stabilizing the system states, a combination with the LQR is further investigated.

This paper is organized as follows. In Section 2, a mathematical model is formulated by employing a first principle approach based on the Newton-Euler equations for the description of the dynamic characteristics of a quadrotor. Section 3 describes the design of the controller and observer based on a polytopic representation. The fourth section introduces the synthesis of the controller and observer gains. The fifth section presents the adapted EKF-LQR method. In Section 6, results are presented with comments before conclusions and an outlook of future work are given in Section 7.

2 Modeling of the Quadrotor

In the literature, research has been conducted to build quadrotor models that take into consideration some parts of the knowledge that humans have acquired about the aerodynamic phenomena, see e.g. [6]. Such models allow designing a corresponding controller using one or a mixture of the control methods that exist in the

literature.

According to [13], we consider the quadrotor in the earth-fixed inertial coordinate frame $(e_{1\mathrm{I}}, e_{2\mathrm{I}}, e_{3\mathrm{I}})$ and body-fixed frame $(e_{1\mathrm{B}}, e_{2\mathrm{B}}, e_{3\mathrm{B}})$ whose origin is at the center of gravity of the quadrotor as shown in Figure 1. The position of the quadrotor is described by its coordinate vector $\mathbf{p}^T = (x, y, z)$. For the rotation from the earth's inertial frame to the body frame, the ZYX convention for roll, pitch, and yaw angles (ϕ, θ, ψ) is chosen. Indeed, there are several existing conventions to describe the transformation based on the successive rotation about these three axes, see e.g. [5].

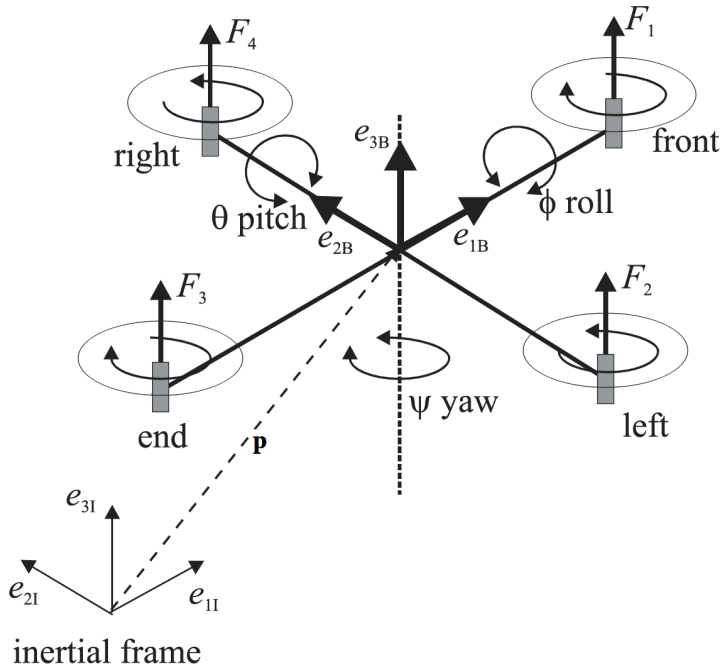

Figure 1: Earth- and body-fixed frame of the quadrotor as introduced in [13].

By applying Newton's law for the rotational and translational motions, the kinematic and dynamic expressions are derived while making the hypothesis that the quadrotor is a rigid body. Considering some assumptions such as neglecting the ground effects and ignoring gyroscopic moments, a set of nonlinear ordinary differential equations is obtained.

After rewriting the previously derived equations into a corresponding state-space form $\dot{\mathbf{x}} = \mathbf{f}(\mathbf{x}, \mathbf{u})$, the model can be decomposed into two parts, as addressed in [13], thus describing the attitude dynamics and the velocity dynamics. However,

in this paper, only the first part is treated according to

$$\begin{cases} \dot{\phi} = \dot{\phi} \\ \ddot{\phi} = \dot{\theta}\dot{\psi}\frac{I_y - I_z}{I_x} - \frac{J_R}{I_x}\dot{\theta}\omega_\mathrm{d} + \frac{l}{I_x}\tau_\phi \\ \dot{\theta} = \dot{\theta} \\ \ddot{\theta} = \dot{\phi}\dot{\psi}\frac{I_z - I_x}{I_y} + \frac{J_R}{I_y}\dot{\phi}\omega_\mathrm{d} + \frac{l}{I_y}\tau_\theta \\ \dot{\psi} = \dot{\psi} \\ \ddot{\psi} = \dot{\phi}\dot{\theta}\frac{I_x - I_y}{I_z} + \frac{l}{I_z}\tau_\psi \ , \end{cases} \tag{1}$$

with the state vector $\mathbf{x} = [\phi, \dot{\phi}, \theta, \dot{\theta}, \psi, \dot{\psi}]^T \in \mathbb{R}^n$ and the input vector $\mathbf{u} = [\tau_\phi, \tau_\theta, \tau_\psi]^T \in \mathbb{R}^m$, representing respectively the roll, pitch, and yaw torque, all depending on the rotor speeds; ω_d is a fictitious disturbance that depends on the speeds of the four rotors, and J_R is the rotor inertia, while I_x, I_y, I_z are the diagonal entries of the quadrotor's inertia matrix.

Using an optimized factorization, where β_1, β_2, and $\beta_3 \in \mathbb{R}$ are free optimization variables, the quasi-linear model

$$\begin{aligned} \underbrace{\begin{bmatrix} \dot{x}_1 \\ \dot{x}_2 \\ \dot{x}_3 \\ \dot{x}_4 \\ \dot{x}_5 \\ \dot{x}_6 \end{bmatrix}}_{\dot{\mathbf{x}}(t)} = & \underbrace{\begin{bmatrix} 0 & 1 & 0 & 0 & 0 & 0 \\ 0 & 0 & 0 & \beta_1 I_1 x_6 & 0 & (1-\beta_1) I_1 x_4 \\ 0 & 0 & 0 & 1 & 0 & 0 \\ 0 & \beta_2 I_2 x_6 & 0 & 0 & 0 & (1-\beta_2) I_2 x_2 \\ 0 & 0 & 0 & 0 & 0 & 1 \\ 0 & (1-\beta_3) I_3 x_4 & 0 & \beta_3 I_3 x_2 & 0 & 0 \end{bmatrix}}_{\mathbf{A}_\mathrm{c}(\mathbf{x}(\mathbf{t}))} \cdot \underbrace{\begin{bmatrix} x_1 \\ x_2 \\ x_3 \\ x_4 \\ x_5 \\ x_6 \end{bmatrix}}_{\mathbf{x}(\mathbf{t})} \\ & + \underbrace{\begin{bmatrix} 0 & 0 & 0 \\ \frac{l}{I_x} & 0 & 0 \\ 0 & 0 & 0 \\ 0 & \frac{l}{I_y} & 0 \\ 0 & 0 & 0 \\ 0 & 0 & \frac{l}{I_z} \end{bmatrix}}_{\mathbf{B}_\mathrm{c}(\mathbf{x}(\mathbf{t}))} \cdot \underbrace{\begin{bmatrix} u_1 \\ u_2 \\ u_3 \end{bmatrix}}_{\mathbf{u}(\mathbf{t})} + \underbrace{\begin{bmatrix} 0 \\ -\frac{J_R}{I_x} x_4 \\ 0 \\ \frac{J_R}{I_y} x_2 \\ 0 \\ 0 \end{bmatrix}}_{\mathbf{G}_\mathrm{c}(\mathbf{x}(\mathbf{t}))} \cdot \omega_\mathrm{d} \end{aligned} \tag{2}$$

has been obtained, where $x_1 \in [\underline{\phi}, \overline{\phi}]$, $x_3 \in [\underline{\theta}, \overline{\theta}]$, $x_5 \in [\underline{\psi}, \overline{\psi}]$, $x_2 \in [\underline{\dot{\phi}}, \overline{\dot{\phi}}]$, $x_4 \in [\underline{\dot{\theta}}, \overline{\dot{\theta}}]$, and $x_6 \in [\underline{\dot{\psi}}, \overline{\dot{\psi}}]$ are assumed to be bounded by a-priori known intervals. Moreover, u_1,u_2,u_3 are respectively the control signals $\tau_\phi, \tau_\theta, \tau_\psi$. The parameters I_1, I_2, and I_3 depend on the inertia matrix entries; $\mathbf{A}_\mathrm{c}$ is the system matrix, $\mathbf{B}_\mathrm{c}$ is the state-independent input matrix, and $\mathbf{G}_\mathrm{c}$ is the disturbance input matrix, coupling the process noise with the system dynamics.

The exploitation of the optimization variables introduced above allows the computation of an adequate system matrix of the quasi-linear realization in each iteration of the control and observer design in the following section to maximize the provable domain of attraction of the operating point (the equilibrium). For further information, where a similar approach was also used for stability analysis, the

reader is referred to [9]. The obtained model in Eq. (2) represents the exact nonlinear dynamics and is used in the simulation as shown in Figure 2 as well as in the controller and observer design phase.

3 Controller and Observer Design

In the obtained model, the appearance of nonlinearities in the system matrix leads to the fact that the separation principle of control and observer design is no longer valid as explained in the paper [10], which means that the controller and observer can influence each other's stability and, therefore, they must be designed simultaneously.

Consider the discrete-time quasi-linear state-space representation

$$\begin{cases} \mathbf{x}_{k+1} = \mathbf{A}(\mathbf{x}_k)\mathbf{x}_k + \mathbf{B}(\mathbf{x}_k)(\mathbf{u}_k + \mathbf{d}_k) + \mathbf{G}_\mathrm{p}\omega_k \\ \mathbf{y}_k = \mathbf{C}\mathbf{x}_k, \end{cases} \tag{3}$$

where $\mathbf{y}_k \in \mathbb{R}^p$, ω_k, and $\mathbf{d}_k \in \mathbb{R}^m$ are respectively the output vector, process noise vector, and actuator fault vector. The faults could manifest themselves in different manners like a blocking, saturation, or efficiency loss of the physical actuators. Finally, $\mathbf{C}$ is the output matrix.

3.1 Design for Model-Based Actuator Fault Compensation

To be able to detect actuator faults, an augmented system model

$$\begin{cases} \underbrace{\begin{bmatrix}\mathbf{x}_{k+1}\\ \mathbf{d}_{k+1}\end{bmatrix}}_{\mathbf{z}_{k+1}} = \underbrace{\begin{bmatrix}\mathbf{A}(\mathbf{x}_k) & \mathbf{B}(\mathbf{x}_k)\\ \mathbf{0}_{(m,n)} & \mathbf{I}_{(m,m)}\end{bmatrix}}_{\mathbf{A}_\mathrm{e}(\mathbf{x}_k)} \cdot \underbrace{\begin{bmatrix}\mathbf{x}_k\\ \mathbf{d}_k\end{bmatrix}}_{\mathbf{z}_k} + \underbrace{\begin{bmatrix}\mathbf{B}(\mathbf{x}_k)\\ \mathbf{0}_{(m,m)}\end{bmatrix}}_{\mathbf{B}_\mathrm{e}(\mathbf{x}_k)} \cdot \mathbf{u}_k + \underbrace{\begin{bmatrix}\mathbf{G_p}\\ \mathbf{0}_{(m,1)}\end{bmatrix}}_{\mathbf{G}_\mathrm{e}} \cdot \omega_k \\ \mathbf{y}_k = \underbrace{\begin{bmatrix}\mathbf{C} & \mathbf{0}_{(p,m)}\end{bmatrix}}_{\mathbf{C}_\mathrm{c}} \cdot \underbrace{\begin{bmatrix}\mathbf{x}_k\\ \mathbf{d}_k\end{bmatrix}}_{\mathbf{z}_k} \end{cases} \tag{4}$$

is formulated by appending a discrete-time integrator disturbance model $\mathbf{d}_{k+1} = \mathbf{d}_k$ for each of the independent faults to the original state vector.

On this basis, a linear time-invariant full-state observer is designed with the discrete-time state-space representation

$$\underbrace{\begin{bmatrix}\hat{\mathbf{x}}_{k+1}\\ \hat{\mathbf{d}}_{k+1}\end{bmatrix}}_{\hat{\mathbf{z}}_{k+1}} = \underbrace{\begin{bmatrix}\tilde{\mathbf{A}} & \tilde{\mathbf{B}}\\ \mathbf{0}_{(m,n)} & \mathbf{I}_{(m,m)}\end{bmatrix}}_{\tilde{\mathbf{A}}_\mathrm{e}} \cdot \underbrace{\begin{bmatrix}\hat{\mathbf{x}}_k\\ \hat{\mathbf{d}}_k\end{bmatrix}}_{\hat{\mathbf{z}}_k} + \underbrace{\begin{bmatrix}\tilde{\mathbf{B}}\\ \mathbf{0}_{(m,m)}\end{bmatrix}}_{\tilde{\mathbf{B}}_\mathrm{e}} \cdot \mathbf{u}_k + \underbrace{\begin{bmatrix}\mathbf{H}_\mathrm{i}\\ \mathbf{H}_\mathrm{f}\end{bmatrix}}_{\mathbf{H}_\mathrm{e}} \cdot \mathbf{C}_\mathrm{e} \cdot (\mathbf{z}_k - \hat{\mathbf{z}}_k), \tag{5}$$

where $\mathbf{H}_\mathrm{e} \in \mathbb{R}^{(n+m)\times p}$ is the constant observer gain; $\tilde{\mathbf{A}}$ and $\tilde{\mathbf{B}}$ are, respectively, the nominal dynamics and input matrices that are chosen in this current paper as the matrices of $\mathbf{A}(\mathbf{x}_k)$ and $\mathbf{B}(\mathbf{x}_k)$ evaluated for the chosen operating point which corresponds to the hovering state.

The estimated states $\hat{\mathbf{z}}_k$ are fed back by the control law

$$\mathbf{u}_k = -\underbrace{\begin{bmatrix}\mathbf{K} & \mathbf{I}_{(m,m)}\end{bmatrix}}_{\mathbf{K}_\mathrm{e}} \cdot \hat{\mathbf{z}}_k, \tag{6}$$

where the multiplication by $\mathbf{K}_\mathrm{e} \in \mathbb{R}^{m\times(m+n)}$ includes the actual state feedback by means of the gain $\mathbf{K}$ and the compensation of the actuator faults.

The architecture of the closed loop is illustrated in Figure 2. For simulation purposes, it has been implemented in Simulink with ode1 as a solver with a small fixed integration step size.

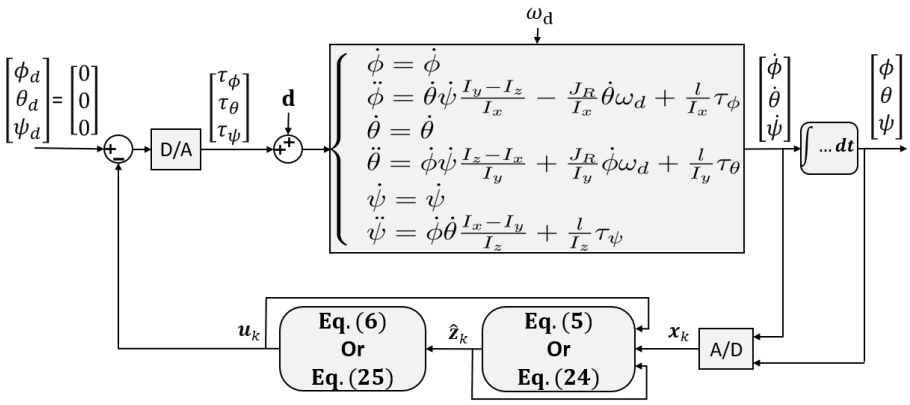

Figure 2: Structure of the linear observer-based state feedback controller

In Figure 2, the block A/D represents the digital-to-analog converter in a first-order-hold mode, and the D/A block is the corresponding analog-to-digital converter.

Considering the error $\mathbf{e}_k = \mathbf{z}_k - \hat{\mathbf{z}}_k$, an augmented closed-loop system representation has been obtained according to

$$\underbrace{\begin{bmatrix}\mathbf{z}_{k+1}\\ \mathbf{e}_{k+1}\end{bmatrix}}_{\mathbf{w}_{k+1}} = \underbrace{\begin{bmatrix}\mathbf{A}(\mathbf{x}_k) - \mathbf{B}(\mathbf{x}_k)\mathbf{K} & \mathbf{B}(\mathbf{x}_k) & \mathbf{B}(\mathbf{x}_k)\mathbf{K} & \mathbf{0}_{(n,m)}\\ \mathbf{0}_{(m,n)} & \xi\cdot\mathbf{I}_{(m,m)} & \mathbf{0}_{(m,n)} & \mathbf{0}_{(m,m)}\\ \mathcal{A}_{31} & (\tilde{\mathbf{B}} - \mathbf{B}(\mathbf{x}_k)) & \mathcal{A}_{33} & \\ \mathbf{0}_{(m,n)} & \mathbf{I}_{(m,m)} & -\mathbf{H}_\mathrm{f}\mathbf{C} & \mathbf{I}_{(m,m)}\end{bmatrix}}_{\mathcal{A}(\mathbf{x}_k)} \cdot \underbrace{\begin{bmatrix}\mathbf{z}_k\\ \mathbf{e}_k\end{bmatrix}}_{\mathbf{w}_k} + \underbrace{\begin{bmatrix}\mathbf{G}_\mathrm{e}\\ \mathbf{G}_\mathrm{e}\end{bmatrix}}_{\mathcal{G}(\mathbf{x}_k)} \cdot \omega_k, \tag{7}$$

with $\mathcal{A}_{31} = \mathbf{A}(\mathbf{x}_k) - \tilde{\mathbf{A}} - (\mathbf{B}(\mathbf{x}_k) - \tilde{\mathbf{B}})\mathbf{K}$ and $\mathcal{A}_{33} = \tilde{\mathbf{A}} - \mathbf{H}_\mathrm{i}\mathbf{C} + (\mathbf{B}(\mathbf{x}_k) - \tilde{\mathbf{B}}(\mathbf{x}_k))\mathbf{K}$.

Remark. To avoid a pure integrator of the actuator fault $\mathbf{d}_k$, a multiplication of the identity matrix by a number $0 < \xi < 1$ is performed during the synthesis stage so that the corresponding mode becomes stabilizable. This parameter choice corresponds to

$$\xi = \begin{cases} 1 & : \text{used for modeling and simulation,} \\ < 1 & : \text{used during synthesis.} \end{cases} \tag{8}$$

Note that this modification only influences the convergence of the following iterative LMI-based control design but leaves the eigenvalues of the closed-loop system model, represented conservatively in a polytopic form, unchanged.

3.2 Simplification of the Augmented System Model for a Control Without Actuator Fault Detection

For the purpose of comparison with the synthesis in which the actuator fault detection is not taken into consideration, the fault $\mathbf{d}_k$ is not estimated and hence not included in the vector $\mathbf{z}_k$ but instead appended to the disturbance vector ω_k. This modification leads to the augmented model

$$\underbrace{\begin{bmatrix} \mathbf{x}_{k+1} \\ \mathbf{e}_{k+1} \end{bmatrix}}_{\mathbf{w}_{k+1}} = \underbrace{\begin{pmatrix} \mathbf{A}(\mathbf{x}_k) - \mathbf{B}(\mathbf{x}_k)\mathbf{K} & \mathbf{B}(\mathbf{x}_k)\mathbf{K} \\ \mathbf{A}(\mathbf{x}_k) - \tilde{\mathbf{A}} - (\mathbf{B}(\mathbf{x}_k) - \tilde{\mathbf{B}})\mathbf{K} & \tilde{\mathbf{A}} - \mathbf{H}_\mathrm{i}\mathbf{C} + (\mathbf{B}(\mathbf{x}_k) - \tilde{\mathbf{B}})\mathbf{K} \end{pmatrix}}_{\mathcal{A}(\mathbf{x}_k)} \cdot \underbrace{\begin{bmatrix} \mathbf{x}_k \\ \mathbf{e}_k \end{bmatrix}}_{\mathbf{w}_k}$$
$$+ \underbrace{\begin{pmatrix} \mathbf{B}(\mathbf{x}_k) & \mathbf{G}_\mathrm{p} \\ \mathbf{B}(\mathbf{x}_k) & \mathbf{G}_\mathrm{p} \end{pmatrix}}_{\mathcal{G}(\mathbf{x}_k)} \cdot \underbrace{\begin{bmatrix} \mathbf{d}_k \\ \omega_k \end{bmatrix}}_{\omega_\mathrm{p}}, \tag{9}$$

which replaces the use of Eq. (7), when required in the following synthesis.

For the same reason, and also during simulation, the fault $\mathbf{d}_k$ is then also removed from $\hat{\mathbf{z}}_k$. Therefore, the state observer that replaces Eq. (5), turns into

$$\hat{\mathbf{x}}_{k+1} = \tilde{\mathbf{A}} \cdot \hat{\mathbf{x}}_k + \tilde{\mathbf{B}} \cdot \mathbf{u}_k + \mathbf{H}_\mathrm{i}\mathbf{C} \cdot (\mathbf{x}_k - \hat{\mathbf{x}}_k), \tag{10}$$

with the simplified control law

$$\mathbf{u}_k = -\mathbf{K} \cdot \hat{\mathbf{x}}_k \tag{11}$$

that replaces Eq. (6).

3.3 Polytopic Uncertainty Representation of the Augmented Closed-Loop System

For control and observer design, the state variables are assumed to be constrained. By chosen limits, the entries of the system matrix and the disturbance input matrix

are also bounded, so that a polytopic domain can be determined to enclose the matrices $\mathcal{A}(\mathbf{x}_k)$ and $\mathcal{G}(\mathbf{x}_k)$ which belong to the convex combination of n_v independent extremal vertex matrices $\mathcal{A}_v$ and $\mathcal{G}_v$ according to

$$[\mathcal{A}(\mathbf{x}_k), \mathcal{G}(\mathbf{x}_k)] \in \left\{ [\mathcal{A}(\zeta), \mathcal{G}(\zeta)] = \sum_{v=1}^{n_v} \zeta_v \cdot [\mathcal{A}_v, \mathcal{G}_v]; \sum_{v=1}^{n_v} \zeta_v = 1; \zeta_v \geq 0 \right\}. \tag{12}$$

Here, ζ_v are the scheduling variables.

During this formulation, identical dependencies in the matrix entries should be identified to reduce the conservativeness of the polytopic model as far as possible.

4 Optimization of the Control and Observer Gains

In the paper [4], the authors have developed an iterative LMI tool that is briefly explained in the following sub-sections. It serves as the basis for the optimization of the gains of the fault-tolerant control structure developed in this paper.

4.1 Eigenvalue Domain Assignment

To realize certain closed-loop characteristics (such as the settling time or maximum overshoot) in combination with robustness against the uncertainty represented by the previous polytopic model, an eigenvalue domain assignment is performed for all extremal system matrices introduced in Eq. (12) with the help of a common Lyapunov function candidate.

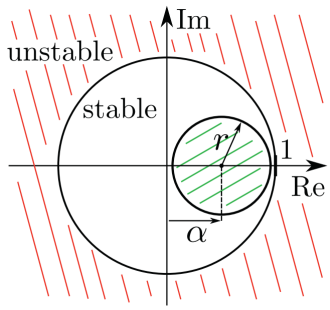

Figure 3: Desired stability domain in the interior of the unit circle of the complex z-plane.

The parameterized sub-region inside the unit circle of the z-plane with radius r and midpoint α, as illustrated in Figure 3, can be expressed according to [4] by the LMI condition

$$\begin{bmatrix} \mathbf{L} & (\mathcal{A}_v - \alpha\mathbf{I}) \\ (\mathcal{A}_v - \alpha\mathbf{I})^T & r^2\mathbf{P} \end{bmatrix} \succ 0, v = 1, ..., n_v. \tag{13}$$

Here, the positive-definite matrix $\mathbf{P} = \mathbf{P}^T$ is a free decision variable and parameterizes a common Lyapunov function for all realizations of the polytopic model. Its inverse, is expressed in terms of $\mathbf{P}^{-1} \succeq 2\hat{\mathbf{P}}^{-1} - \hat{\mathbf{P}}^{-1}\mathbf{P}\hat{\mathbf{P}}^{-1} =: \mathbf{L}$. This approximation has been obtained by a linearization approach using a first-order Neumann series, cf. [3].

In the absence of stochastic noise, a successful solution of Eq. (13) ensures asymptotic stability of the observer-based closed-loop control structure. This solution can be obtained by means of the first algorithm in [4], in which the matrix $\mathbf{P}$ is updated in each iteration step l. Ending with admissible values for r_{end} (typically a predefined value) and α, leading to stability domains in the interior of the unit circle, a preliminary controller and observer design is obtained.

4.2 Desensitization Towards Noise

In the presence of stochastic noise, the solution of Sec. 4.1 is improved in the sense of desensitization towards noise. For that purpose, the discrete-time version of the Itô differential operator has been used to expand the Lyapunov conditions and to express the size of the domain around the equilibrium for which stability cannot be proven due to noise excitation. After some mathematical reformulation, an iteration rule for the optimization task has been derived in [4] that uses a cost function subject to LMI constraints in the form

$$\min J = \sum_{v=1}^{n_v} \frac{\text{trace}\{\mathbf{N}\}}{\det(-\hat{\mathbf{M}}_v)}, \tag{14}$$

with

$$\mathbf{P} \succ 0, \tag{15}$$

$$\mathbf{N} \succ 0, \tag{16}$$

$$\begin{bmatrix} \mathbf{L} & \mathcal{G}_v \\ \mathcal{G}_v^T & \mathbf{N} \end{bmatrix} \succ 0, v = 1, ..., n_v, \tag{17}$$

$$\begin{bmatrix} \mathbf{L} & (\mathcal{A}_v - \alpha\mathbf{I}) \\ (\mathcal{A}_v - \alpha\mathbf{I})^T & r^2\mathbf{P} \end{bmatrix} \succ 0, v = 1, ..., n_v, \tag{18}$$

and $\hat{\mathbf{M}}_v = \hat{\mathcal{A}}_v^T \hat{\mathbf{P}} \hat{\mathcal{A}}_v - \hat{\mathbf{P}}$, where the optimization variables β_1, β_2, and β_3 introduced in Eq. (2) are included as further decision variables. The free matrix variable $\mathbf{N}$ is automatically determined by means of an LMI solver so that $\mathbf{N} \succeq \mathcal{G}_v^T \mathbf{P} \mathcal{G}_v$ holds for all $v = 1, ..., n_v$.

In all expressions in this subsection, the symbol $\hat{(\cdot)}$ means the updated variable from the previous iteration.

Note that a successful minimization of the cost function in Eq. (14) leads to a reduction of sensitivity of the closed-loop system against noise, as it has been originally derived in [10], [11], and [4].

4.3 Summary of the Design Procedure

The procedure to find suitable controller and observer gains and to optimize their numerical values according to the desensitization criteria described in the previous subsection is summarized in the following Nassi-Shneiderman diagram.

Construction of the nonlinear system model Eq. (1)
Derive the quasi-linear model according to Eq. (2)
Discretization using the explicit Euler method
Build the polytopic domain of Eq. (12) for the augmented closed-loop model in Eq. (7)
Initialization with $r = 2$ and the step size $\Delta r = 0.2$ and $\hat{\mathbf{P}}_0^{-1} = \mathbf{I}$, Here: use a fixed value $\alpha = 0$
while $r > r_{\text{end}}$
Decrease $r := r - \Delta r$
Generate Eqs. (2), (7)
Compute the gains $\mathbf{K}$, $\mathbf{H}_{\text{i}}$ and $\mathbf{H}_{\text{f}}$, and the matrix $\mathbf{P}$ by solving the LMI in Eq. (13)
Checking the feasibility
Feasible: Update $\hat{\mathbf{P}}$ and store the matrices
Infeasible: Re-increase $r := r + \Delta r$ and reduce Δr by half
Initialization with the most recent successfully computed matrices obtained from the previous part of the algorithm
Keep r_{end} and $\alpha = 0$ fixed and initialize $\hat{\mathbf{M}}_v = \mathbf{I}$
while $\text{trace}(\mathbf{N}_l) - \text{trace}(\mathbf{N}_{l-1}) > 10^{-7}$
Generate Eqs. (2), (7)
Optimize the cost function in Eq. (14) subject to Eqs. (15), (16), (17), (18)
Update $\hat{\mathbf{P}}^{-1}$ and $\hat{\mathbf{M}}_v$ if an admissible solution has been found, and store the matrices
Use the final controller and observer gains in the closed-loop structure shown in Figure 2

Remark. In this work, the construction of the polytopic representation as seen in the diagram above is made only by a choice of intervals for the state variables. Uncertainty of the system parameters (e.g. the inertia) can be included analogously, leading to an increase in the number of vertices.

5 Alternative Control Parametrization: Extended Kalman Filter-Based Linear Quadratic Regulator Design

In order to analyze the efficiency of the iterative LMI-based method, an LQR approach is implemented additionally that uses states and actuator fault estimates obtained from an EKF as a stochastic filter approach applicable to nonlinear systems. Such an approach does not prove stability in contrast to the iterative LMI-based approach.

5.1 The Extended Kalman Filter

An extension of Eq. (3) with additive Gaussian system and measurement noise $\mathbf{w}_k$ and $\mathbf{v}_k$ is given as

$$\begin{cases} \mathbf{x}_{k+1} = \mathbf{A}(\mathbf{x}_k)\mathbf{x}_k + \mathbf{B}(\mathbf{x}_k)(\mathbf{u}_k + \mathbf{d}_k) + \mathbf{G}_\mathrm{p}\omega_k + \mathbf{W}\mathbf{w}_k \\ \mathbf{y}_k = \mathbf{C}\mathbf{x}_k + \mathbf{v}_k \\ \mathbf{d}_{k+1} = \mathbf{d}_k + \mathbf{E}\mathbf{g}_k, \end{cases} \tag{19}$$

with their expected mean values and covariance matrices $\mu_{\mathbf{w},k} = 0$, $\mathbb{C}_\mathbf{w}$, $\mu_{\mathbf{v},k} = 0$ and $\mathbb{C}_\mathbf{v}$. Here, $\mathbf{W}$ is the additive disturbance input matrix.

To be able to detect actuator faults, an augmented system model

$$\begin{cases} \underbrace{\begin{bmatrix}\mathbf{x}_{k+1}\\ \mathbf{d}_{k+1}\end{bmatrix}}_{\mathbf{z}_{k+1}} = \underbrace{\begin{bmatrix}\mathbf{A}(\mathbf{x}_k) & \mathbf{B}(\mathbf{x}_k)\\ \mathbf{0}_{(m,n)} & \mathbf{I}_{(m,m)}\end{bmatrix}}_{\mathbf{A}_\mathrm{e}(\mathbf{x}_k)} \cdot \underbrace{\begin{bmatrix}\mathbf{x}_k\\ \mathbf{d}_k\end{bmatrix}}_{\mathbf{z}_k} + \underbrace{\begin{bmatrix}\mathbf{B}(\mathbf{x}_k)\\ \mathbf{0}_{(m,m)}\end{bmatrix}}_{\mathbf{B}_\mathrm{e}(\mathbf{x}_k)} \cdot \mathbf{u}_k \\ \qquad + \underbrace{\begin{bmatrix}\mathbf{G}_\mathrm{p} & \mathbf{W} & \mathbf{0}_{(n,m)}\\ \mathbf{0}_{(m,1)} & \mathbf{0}_{(m,n)} & \mathbf{E}\end{bmatrix}}_{\mathbf{G}_\mathrm{d}} \cdot \begin{bmatrix}\omega_k\\ \mathbf{w}_k\\ \mathbf{g}_k\end{bmatrix} \\ \mathbf{y}_k = \underbrace{\begin{bmatrix}\mathbf{C} & \mathbf{0}_{(p,m)}\end{bmatrix}}_{\mathbf{C}_\mathrm{e}} \cdot \underbrace{\begin{bmatrix}\mathbf{x}_k\\ \mathbf{d}_k\end{bmatrix}}_{\mathbf{z}_k} \end{cases} \tag{20}$$

is formulated by appending discrete-time integrator disturbance models to the original state vector, where $\mathbf{E}$ is the input matrix of the additive actuator faults and $\mathbf{g}_k$ is a noise term representing their dynamics by an additive Gaussian noise process; $\mathbb{C}_\mathbf{g}$ is its covariance matrix.

The EKF approach consists of two parts. In the prediction part, the prior mean and covariance are computed according to

$$\underbrace{\begin{bmatrix}\mu^\mathrm{p}_{\mathbf{x},k}\\ \mu^\mathrm{p}_{\mathbf{d},k}\end{bmatrix}}_{\mu^\mathrm{p}_{\mathbf{z},k}} = \begin{bmatrix}\mathbf{A}(\mu^\mathrm{e}_{\mathbf{x},k-1}) & \mathbf{0}_{(n,m)}\\ \mathbf{0}_{(m,n)} & \mathbf{I}_{(m,m)}\end{bmatrix} \cdot \underbrace{\begin{bmatrix}\mu^\mathrm{e}_{\mathbf{x},k-1}\\ \mu^\mathrm{e}_{\mathbf{d},k-1}\end{bmatrix}}_{\mu^\mathrm{e}_{\mathbf{z},k-1}} + \begin{bmatrix}\mathbf{B}(\mu^\mathrm{e}_{\mathbf{x},k-1})\\ \mathbf{0}_{(m,m)}\end{bmatrix} \cdot (\mathbf{u}_k + \mu^\mathrm{e}_{\mathbf{d},k-1}), \tag{21}$$

and

$$\mathbb{C}^{\mathrm{p}}_{\mathbf{z},k} = \underbrace{\begin{bmatrix} \tilde{\mathbf{A}} & \tilde{\mathbf{B}} \\ \mathbf{0}_{(m,n)} & \mathbf{I}_{(m,m)} \end{bmatrix}}_{\tilde{\mathbf{A}}_{\mathrm{e}}} \cdot \mathbb{C}^{\mathrm{e}}_{\mathbf{z},k-1} \cdot \underbrace{\begin{bmatrix} \tilde{\mathbf{A}} & \tilde{\mathbf{B}} \\ \mathbf{0}_{(m,n)} & \mathbf{I}_{(m,m)} \end{bmatrix}^T}_{\tilde{\mathbf{A}}_{\mathrm{e}}^T} + \mathbf{G}_{\mathrm{d}} \cdot \begin{bmatrix} \mathbb{C}_{\omega} & \mathbf{0}_{(1,n)} & \mathbf{0}_{(1,m)} \\ \mathbf{0}_{(n,1)} & \mathbb{C}_{\mathbf{w}} & \mathbf{0}_{(n,m)} \\ \mathbf{0}_{(m,1)} & \mathbf{0}_{(m,n)} & \mathbb{C}_{\mathbf{g}} \end{bmatrix} \cdot \mathbf{G}_{\mathrm{d}}^T. \tag{22}$$

In the equation above, $\tilde{\mathbf{A}}$ and $\tilde{\mathbf{B}}$ are, respectively, the nominal dynamics and input matrices that are chosen in this current paper as the matrices of $\mathbf{A}(\mathbf{x}_k)$ and $\mathbf{B}(\mathbf{x}_k)$ evaluated for the chosen operating point which corresponds to the hovering state. Here, $\mathbb{C}_{\omega}$ is the variance of the process noise that reflects the influence of the rotor speed-dependent nonlinearity in the system model. The superscripts $(.)^{\mathrm{p}}$ and $(.)^{\mathrm{e}}$, respectively, denote the computed prior and posterior values with respect to the current measurement.

The second part is the update of the predicted mean and covariance in the innovation stage which starts with the computations of the Kalman gain

$$\mathbf{L}_k = \mathbb{C}^{\mathrm{p}}_{\mathbf{z},k} \cdot \mathbf{C}_{\mathrm{e}}^T \cdot (\mathbf{C}_{\mathrm{e}} \cdot \mathbb{C}^{\mathrm{p}}_{\mathbf{z},k} \cdot \mathbf{C}_{\mathrm{e}}^T + \mathbb{C}_{\mathbf{v}})^{-1}. \tag{23}$$

Then, estimates for the states and actuator faults are obtained with the following equation

$$\mu^{\mathrm{e}}_{\mathbf{z},k} = \mu^{\mathrm{p}}_{\mathbf{z},k} + \mathbf{L}_k \cdot (\mathbf{C}\mathbf{x}_k - \mathbf{C}_{\mathrm{e}}\mu^{\mathrm{p}}_{\mathbf{z},k}), \tag{24}$$

besides its corresponding covariance

$$\mathbb{C}^{\mathrm{e}}_{\mathbf{z},k} = (\mathbf{I}_{(n+m,n+m)} - \mathbf{L}_k\mathbf{C}_{\mathrm{e}}) \cdot \mathbb{C}^{\mathrm{p}}_{\mathbf{z},k}, \tag{25}$$

which are both fed back to the prediction part to be used for the next step.

5.2 The Linear Quadratic Regulator

For the control implementation, the mean value of the state estimates obtained in Eq. (24) is fed back by using the control law

$$\mathbf{u}_k = -\underbrace{\begin{bmatrix} \mathbf{K} & \mathbf{I}_{(m,m)} \end{bmatrix}}_{\mathbf{K}_{\mathrm{e}}} \cdot \mu^{\mathrm{e}}_{\mathbf{z},k}, \tag{26}$$

where the controller gain

$$\mathbf{K} = (\tilde{\mathbf{B}}^T\mathbf{S}\tilde{\mathbf{B}} + \mathbf{R})^{-1} \cdot (\tilde{\mathbf{B}}^T\mathbf{S}\tilde{\mathbf{A}}) \tag{27}$$

depends on the matrix $\mathbf{S}$ obtained by solving the algebraic Riccati equation

$$\tilde{\mathbf{A}}^T\mathbf{S}\tilde{\mathbf{A}} - \mathbf{S} - (\tilde{\mathbf{A}}^T\mathbf{S}\tilde{\mathbf{B}}) \cdot (\tilde{\mathbf{B}}^T\mathbf{S}\tilde{\mathbf{B}} + \mathbf{R})^{-1} \cdot (\tilde{\mathbf{B}}^T\mathbf{S}\tilde{\mathbf{A}}) + \mathbf{Q} = \mathbf{0}_{(n,n)}. \tag{28}$$

The positive-definite symmetric matrices $\mathbf{R}$ and $\mathbf{Q}$ are the weighting matrices chosen by a trial-and-error approach for the cost function

$$J(\mathbf{u}_k) = \sum_{k=1}^{\infty} (\mathbf{x}_k^T \mathbf{Q} \mathbf{x}_k + \mathbf{u}_k^T \mathbf{R} \mathbf{u}_k) \tag{29}$$

to be minimized.

6 Simulation Results

This section presents the simulation results of the quadrotor model as shown in Figure 2 with the nominal matrices corresponding to the hovering state. The sample time for discretization is set to 1 ms. The initial states are set to $\pi/4$ rad for each angle. As a control goal, the desired hovering state $[\phi_\mathrm{d}, \theta_\mathrm{d}, \psi_\mathrm{d}]^T = [0, 0, 0]^T$ shall be reached.

For the LMI-based approach, the eigenvalue locations are determined by the predefined sub-circle that is chosen with α as the origin of the z-plane and $r_\mathrm{end} = 0.999$. For the LQR, the weighting matrices are chosen as $\mathbf{R} = \mathrm{diag}([2, 2, 2])$ and $\mathbf{Q} = \mathrm{diag}([50, 10, 50, 10, 50, 10])$.

The values of the parameters that were used are listed in Table 1.

Table 1: Values of the parameters of the quadrotor model.

Parameter	Values
l [m]	0.2
J_R [kg·m^2]	$3.36{\cdot}10^{-5}$
$I_x{=}I_y$ [kg·m^2]	$4.85{\cdot}10^{-3}$
I_z [kg·m^2]	$8.81{\cdot}10^{-3}$
m [kg]	0.5

6.1 Simulation Without Output Noise and Without Detection of Actuator Faults

In the first stage, the simulation was made without taking into consideration any disturbances $\omega_k = 0$. Moreover, also the detection of the actuator faults was deactivated. After 3 seconds, an actuator fault occurs, which leads to a deviation in the yaw torque τ_ψ of -12 Nm and in the pitch torque τ_ϕ with -9 Nm.

Figure 4 shows a convergence to the steady hovering state after the initial deviation within the first 3 s. At $t = 3$ s, the occurrence of the actuator fault causes a deviation with an oscillatory behavior of the roll and pitch angles before ending in a non-desired attitude and orientation. The same figure shows the temporal evolution of the roll, pitch, and yaw torques. After the time of 3 s, they show a

strong oscillation before converging to zero, however, without bringing the system to the desired goal.

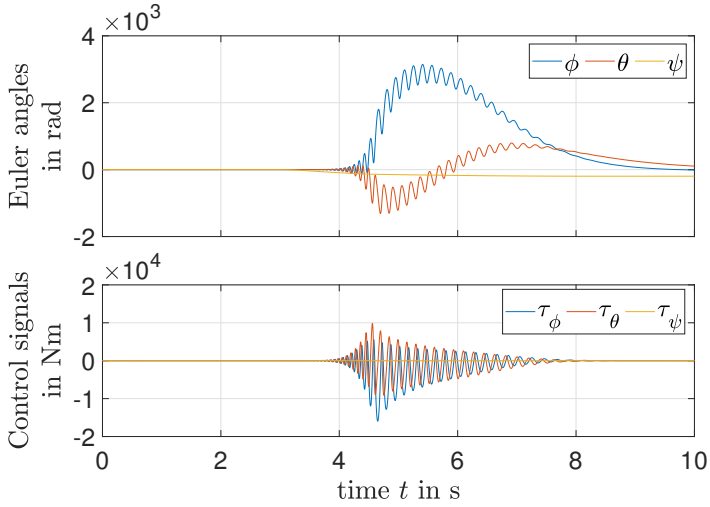

Figure 4: Regulation of the quadrotor's attitude without actuator fault detection

6.2 Simulation With Output Noise and With Compensation of Actuator Faults

To evaluate the robustness against the disturbances, a Gaussian distributed random process noise was taken into consideration with the standard deviation matrix $\mathbf{G}_{\mathrm{e}}$ in Eq. (4), together with a Gaussian distributed measurement noise with a mean of 0 and a standard deviation of $\frac{\pi}{1200}$ rad. The same actuator fault magnitude as in Sec. 6.1 is applied in the current section.

The bounds chosen for the angular velocity states specified in rad/s are $\dot{\theta} \in [-8\pi, 8\pi]$, $\dot{\phi} \in [-8\pi, 8\pi]$, $\dot{\psi} \in [-8\pi, 8\pi]$.

Figure 5 shows a convergence in a short time for the Euler angles even with the stochastic noise in response to the initial states. The deviations of the angular velocities caused by the actuator fault remain within the predefined bounds as seen in Figure 6. The associated control signals are shown in the same Figure.

6.3 Simulation with LQR based on an EKF

With the same noise used for the simulation of the iterative LMI-based method, and choosing $\mathbb{C}_{\omega} = 5$, $\mathbb{C}_{\mathbf{g}} = \mathrm{diag}([10, 10, 10])$, $\mathbb{C}_{\mathbf{v}} = \mathrm{diag}([4, 4, 4])$, and $\mathbb{C}_{\mathbf{w}} = \mathrm{diag}([2, 2, 2, 2, 2, 2])$ besides initializing the filter with $\mathbb{C}_{\mathbf{d},0} = \mathrm{diag}([10, 10, 10])$ and

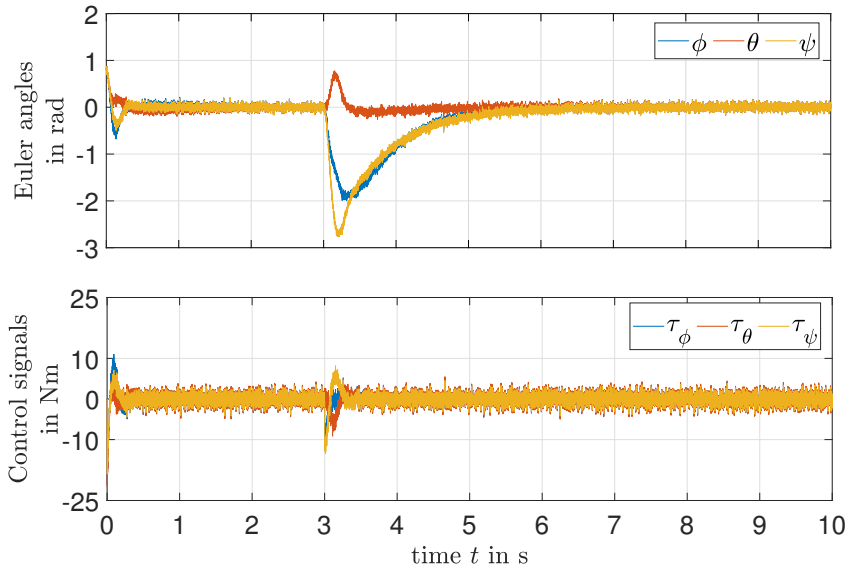

Figure 5: Regulation of the quadrotor's attitude in the presence of Gaussian output noise and actuator faults.

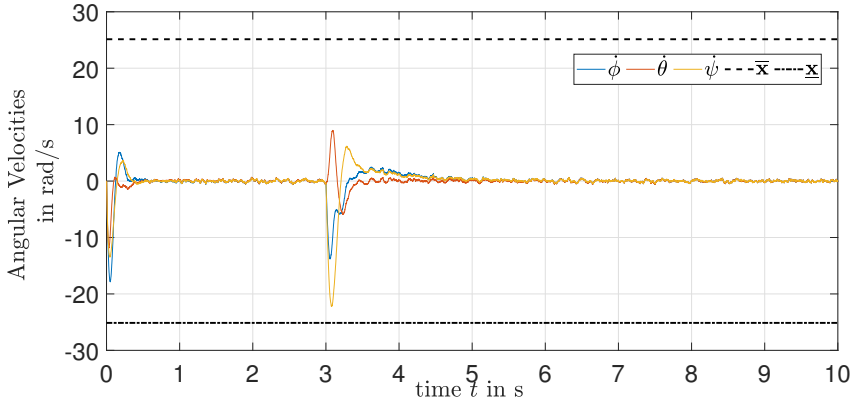

Figure 6: Response of the quadrotor's angular velocities in the presence of Gaussian output noise and actuator faults

$\mathbb{C}_{\mathbf{x},0} = \text{diag}([80, 50, 80, 50, 80, 50])$, a simulation of the attitude response and the corresponding control signals is obtained.

Figure 7 depicts the convergence of the Euler angles in a smooth way in response

to the initial states. After the actuator fault at 3s, the state variables converge within 2s but with a larger amplitude deviation than obtained for the robust LMI solution. The same Figure shows the corresponding control signals.

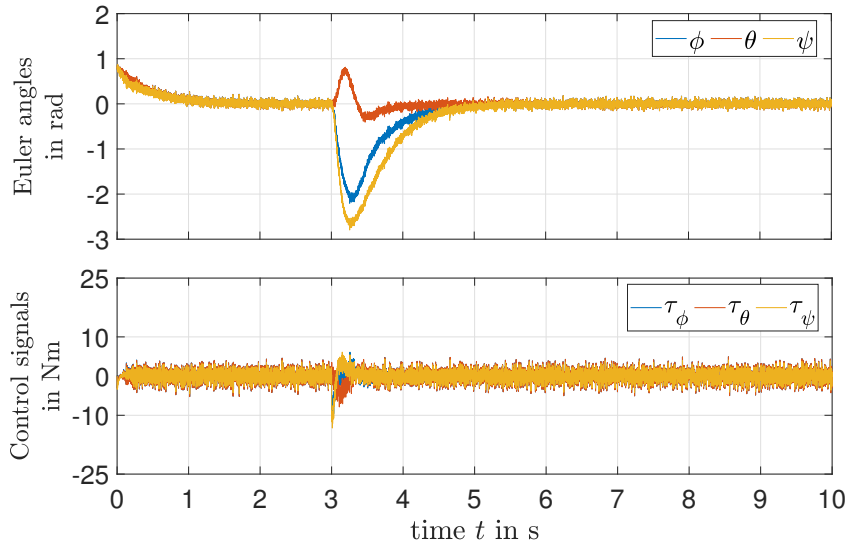

Figure 7: Regulation of the quadrotor's attitude in the presence of Gaussian output noise and actuator faults with EKF-based LQR method

In summary, the response of the LMI-based method takes a shorter time to converge compared with the EKF-based LQR. Additionally, dealing with the actuator fault was better. Due to the fact that the filter gain needs to be recomputed in the update step of the EKF-based LQR, in contrast to time-invariant gains in the LMI-based method, the novel approach helps to significantly reduce the computational effort despite its inherent proof of stability over the operating domain chosen for the parameterization of the polytopic uncertainty model.

7 Conclusions and Outlook on Future Work

The computation of controller and observer gains taking into consideration actuator faults, process noise, and nonlinearities has been possible thanks to the developed iterative LMI approach. In addition to the guaranteed stability, satisfactory time domain behavior has been achieved by a choice of the location of the eigenvalues within the z-plane. The resulting time-domain performance outperformed the one obtained with the EKF-based LQR method which in addition does not inherit a proof of stability for nonlinear models and includes much more parameters to tune.

Although the computation for the iterative LMI-based approach is made offline, attention should be paid to the computational effort. It may turn into an issue if the order of the closed loop and the number of uncertain parameters become larger. To overcome such an obstacle, the following paths can be investigated in future work: On the one hand, the pure polytopic uncertainty model can be replaced by a norm-bounded one. On the other hand, to reduce the conservativeness of the realizations, Chebyshev points can be determined for determining tighter enclosures of nonlinear dependencies. Fundamental work in this direction is published in [14]. Finally, research on using a flatness-based approach for the computation of a feedforward control together with a feedback linearization of the nonlinear plant with nominal parameters is promising to reduce the width of the polytopic domain that needs to be stabilized by a robust feedback controller.

References

[1] Blanke, M., Kinnaert, M., Lunze, J., and Staroswiecki, M., editors. *Diagnosis and fault-tolerant control*. Springer, Berlin; New York, 2nd edition, 2006. DOI: 10.1007/978-3-540-35653-0.

[2] Chan Shi, J. and Dwi, P. Fault detection and identification in Quadrotor system (Quadrotor robot). In *2016 IEEE International Conference on Automatic Control and Intelligent Systems (I2CACIS)*, pages 11–16, Selangor, Malaysia, 2016. IEEE. DOI: 10.1109/I2CACIS.2016.7885281.

[3] Dehnert, R. *Entwurf robuster Regler mit Ausgangsrückführung für zeitdiskrete Mehrgrößensysteme*. Business, Economics, and Law. Springer Fachmedien, Wiesbaden, 2020. DOI: 10.1007/978-3-658-29900-2.

[4] Dehnert, R., Damaszek, M., Lerch, S., Rauh, A., and Tibken, B. Robust feedback control for discrete-time systems based on iterative LMIs with polytopic uncertainty representations subject to stochastic noise. *Frontiers in Control Engineering*, 2:786152, 2022. DOI: 10.3389/fcteg.2021.786152.

[5] Diebel, J. Representing attitude: Euler angles, unit quaternions, and rotation vectors. *Matrix*, 58(15–16):1–35, 2006. URL: https://www.astro.rug.nl/software/kapteyn-beta/_downloads/attitude.pdf, accessed on June 20, 2023.

[6] Hoffmann, G., Huang, H., Waslander, S., and Tomlin, C. Quadrotor helicopter flight dynamics and control: Theory and experiment. In *AIAA Guidance, Navigation and Control Conference and Exhibit*, Hilton Head, South Carolina, 2007. American Institute of Aeronautics and Astronautics. DOI: 10.2514/6.2007-6461.

[7] Patton, R. and Klinkhieo, S. Actuator fault estimation and compensation based on an augmented state observer approach. In *Proceedings of the 48h*

IEEE Conference on Decision and Control (CDC) held jointly with 2009 28th Chinese Control Conference, pages 8482–8487, Shanghai, China, 2009. IEEE. DOI: 10.1109/CDC.2009.5399548.

[8] Raja, M. M. Extended Kalman Filter and LQR controller design for quadrotor UAVs. Master's thesis, Wright State University, 2017. URL: https://corescholar.libraries.wright.edu/etd_all/1761, accessed on June 20, 2023.

[9] Rauh, A., Bourgois, A., and Jaulin, L. Verifying provable stability domains for discrete-time systems using ellipsoidal state enclosures. *Acta Cybernetica*, pages 267–291, 2022. DOI: 10.14232/actacyb.293871.

[10] Rauh, A., Dehnert, R., Romig, S., Lerch, S., and Tibken, B. Iterative solution of linear matrix inequalities for the combined control and observer design of systems with polytopic parameter uncertainty and stochastic noise. *Algorithms*, 14(7):205, 2021. DOI: 10.3390/a14070205.

[11] Rauh, A. and Romig, S. Linear matrix inequalities for an iterative solution of robust output feedback control of systems with bounded and stochastic uncertainty. *Sensors*, 21(9):3285, 2021. DOI: 10.3390/s21093285.

[12] Telbissi, K. and Benzaouia, A. Robust fault tolerant control for uncertain switched systems with time delay. *Journal of Control, Automation and Electrical Systems*, 2023. DOI: 10.1007/s40313-022-00983-2.

[13] Voos, H. Nonlinear state-dependent Riccati equation control of a quadrotor UAV. In *2006 IEEE Conference on Computer Aided Control System Design, 2006 IEEE International Conference on Control Applications, 2006 IEEE International Symposium on Intelligent Control*, pages 2547–2552, Munich, Germany, 2006. IEEE. DOI: 10.1109/CACSD-CCA-ISIC.2006.4777039.

[14] Warthenpfuhl, S. A. and Tibken, B. Guaranteed bounds for robust LMI problems with polynomial parameter dependence. *IFAC Proceedings Volumes*, 41(2):10057–10062, 2008. DOI: 10.3182/20080706-5-KR-1001.01702.

[15] Xu, Y., Yuan, X., and Zhu, J. EKF-LQR-based cooperative optimal control of IPMSM. In *Proceedings of the 9th International Conference on Computer and Automation Engineering*, pages 307–312, Sydney Australia, 2017. ACM. DOI: 10.1145/3057039.3057075.

[16] Yu, X.-H. Actuator fault compensation for a helicopter model. In *Proceedings of 2003 IEEE Conference on Control Applications*, Volume 2, pages 1372–1374, Istanbul, Turkey, 2003. IEEE. DOI: 10.1109/CCA.2003.1223212.